J|A|C|S ARTICLES

Published on Web 03/11/2009

Electron Transfer Across Multiple Hydrogen Bonds: The Case of Ureapyrimidinedione-Substituted Vinyl Ruthenium and Osmium Complexes

Markus Pichlmaier,[†] Rainer F. Winter,*[,†] Manfred Zabel,[†] and Stanislav Záliš*[,‡]

Institut für Anorganische Chemie der Universität Regensburg, D-93040 Regensburg, Germany, and J. Heyrovský Institute of Physical Chemistry, v.v.i, Academy of Sciences of the Czech Republic, Czech Republic

Received December 16, 2008; E-mail: rainer.winter@chemie.uni-regensburg.de; stanislav.zalis@jh-inst.cas.cz

Abstract: Ruthenium and osmium complexes **2a**,**b** and **3a**,**b** featuring the *N*-4,6-dioxo-5,5-dibutyl- or the *N*-4,6-dioxo-5,5-di-(2-propenyl)-1,4,5,6-tetrahydropyrimidin-2-yl-*N*′(4-ethenylphenyl)-urea ligand dimerize by a self-complementary quadruply hydrogen-bonding donor/donor/acceptor/acceptor (DDAA) motif. We provide evidence that the dimeric structures are maintained in nonpolar solvents and in 0.1 M NBu_4PF_6/CH_2Cl_2 supporting electrolyte solution. All complexes are reversibly oxidized in two consecutive *two-electron* oxidations ($\Delta E_{1/2} \approx 500$ mV) without any discernible potential splitting for the oxidation of the individual hydrogen-bridged redox active moieties. IR and UV/vis/NIR spectroelectrochemistry show a one-step conversion of the neutral to the dication without any discernible features of an intermediate monooxidized radical cation. Oxidation-induced IR changes of the NH and CO groups that are involved in hydrogen bonding are restricted to the styryl-bonded urea NH function. IR band assignments are aided by quantum chemical calculations. Our experimental findings clearly show that, at least in the present systems, the ureapyrimidinedione (Upy) DDAA hydrogen-bonding motif does not support electron transfer. The apparent reason is that neither of the hydrogen-bonding functionalities contributes to the occupied frontier levels. This results in nearly degenerate pairs of MOs representing the in-phase and out-of-phase combinations of the individual monomeric building blocks.

Introduction

Electron transfer is one of the most fundamental processes in chemistry and biology. The spatial organization of the electron donor and the electron acceptor in proteins, peptides, and enzymes as well as the rate of electron transfer between them critically depends on the structure-directing and charge-transmitting properties of hydrogen bridges[1−5] as is exemplified by photosystem II[6,7] and cytochrome *c*.[8,9] The search for strong, multiple hydrogen bridges as a tool for the directed organization of matter in synthetical supramolecular systems has led to the elaboration of several new and interesting motifs. Among these, the self-complementary DDAA arrangement of two hydrogen bond donor (D) and acceptor (A) sites as it is present in ureapyrimidones or urea-*s*-triazines has been a particular success story.[10−13] Self-complementary quadruple hydrogen bridges lead to high association constants of $\sim 10^5-10^7$ in apolar solvents. This has allowed for the formation of hydrogen-bonded linear or cross-linked macrocycles,[14] and of oligomers or polymers that reversibly assemble or disintegrate upon changing the polarity and hydrogen-bonding capability of the surrounding medium.[13−17] One disadvantage of the latter systems is the frequently observed formation of complex equilibria involving different interconverting tautomers with hard-to-predict tautomer

[†] Institut für Anorganische Chemie der Universität Regensburg.
[‡] J. Heyrovský Institute of Physical Chemistry, v.v.i, Academy of Sciences of the Czech Republic.

(1) Gray, H. B.; Winkler, J. R. In *Electron Transfer in Chemistry and Biology*; Balzani, V., Ed.; Wiley-VCH: Weinheim, 2001; Vol. 1, p 3.
(2) Antonello, S.; Formaggio, F.; Moretto, A.; Toniolo, C.; Maran, F. *J. Am. Chem. Soc.* **2003**, *125*, 2874–2875.
(3) Serron, S. A.; Aldridge, W. S., III; Fleming, C. N.; Danell, R. M.; Baik, M.-H.; Sykora, M.; Dattelbaum, D. M.; Meyer, T. J. *J. Am. Chem. Soc.* **2004**, *126*, 14506–14514.
(4) Kümmerle, R.; Kyritsis, P.; Gaillard, J.; Moulis, J.-M. *J. Inorg. Biochem.* **2000**, *79*, 83–91.
(5) Stubbe, J.; Nocera, D.; Yee, C. S.; Chang, M. C. Y. *Chem. Rev.* **2003**, *103*, 2167–2202.
(6) Zhang, C. *Biochim. Biopphys. Acta, Bioenerg.* **2007**, *1767*, 493–499.
(7) Semin, B. K.; Lovyagina, E. R.; Timofeev, K. N.; Ivanov, I. I.; Rubin, A. B.; Seibert, M. *Biochemistry* **2005**, *44*, 9746–9757.
(8) Liu, H.; Yamamoto, H; J, Wei; Waldeck, D. H. *Langmuir* **2003**, *19*, 2378–2387.
(9) Langen, R.; Colón, J. L.; Casimiro, D. R.; Karpishin, T. B.; Winkler, J. R.; Gray, H. B. *J. Biol. Inorg. Chem.* **1996**, *1*, 221–225.
(10) Beijer, F. H.; Sijbesma, R. P.; Kooijman, H.; Spek, A. L.; Meijer, E. W. *J. Am. Chem. Soc.* **1998**, *120*, 6761–6769.
(11) Sijbesma, R. P.; Meijer, E. W. *Chem. Commun.* **2003**, 5–16.
(12) Corbin, P. S.; Zimmerman, S. C. *J. Am. Chem. Soc.* **1998**, *120*, 9710–9711.
(13) Schmuck, C.; Wienand, W. *Angew. Chem., Int. Ed.* **2001**, *40*, 4363–4369.
(14) Hirschberg, J. H. H. K.; Koevoets, R. A.; Sijbesma, R. P.; Meijer, E. W *Chem. Eur. J.* **2003**, *9*, 4222–4231.
(15) Binder, W. H.; Zirbs, R. Supramolecular Polymers and Networks with Hydrogen Bonds in the Main- and Side-Chain. In *Hydrogen Bonded Polymers*; Binder, W., Ed.; SpringerLink: Heidelberg, 2007; Vol. 207, pp 1−78.
(16) Vázquez-Campos, S.; Crego-Calama, M.; Reinhoudt, D. N. *Supramol. Chem.* **2007**, *19*, 95–106.
(17) Sherrington, D. C.; Taskinen, K. A. *Chem. Soc. Rev.* **2001**, *30*, 83–93.

10.1021/ja809566g CCC: $40.75

Chart 1. Degenerate Tautomerism and Dimerization of *N*-5,5-Dialkyl-4,6-dioxo-1,4,5,6-tetrahydropyrimidin-2-yl-urea derivatives[a]

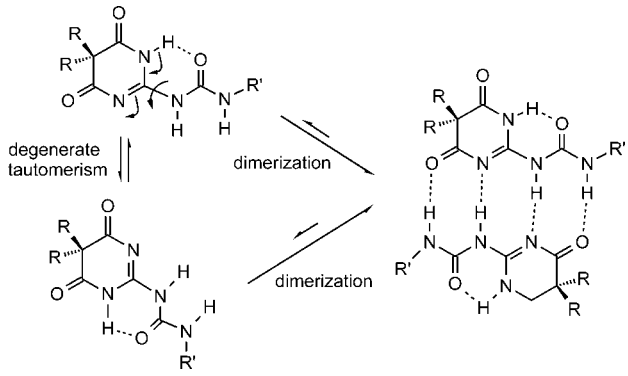

[a] The singly oxidized form of a ferrocenyl substituted dimer (R′ = ferrocenyl) shows borderline class II/III mixed-valent behaviour.[23]

distributions.[12,18] Symmetrically substituted 5,5-dialkyl-4,6-dioxo-1,4,5,6-tetrahydro-pyrimidin-2-yl-urea derivatives have finally resolved the problem of nondegenerate tautomerism (Chart 1).[19]

Ureido-*s*-triazine-bridged assemblies of various oligo(phenylenevinylene) donors and the perylene bisimide acceptor[20] and noncovalently bonded dimers of amidinium-substituted metalloporphyrins[21] or tetrathiofulvalenes[22] and a fullerene-substituted benzoate provide intriguing examples of efficient photochemically triggered electron transfer from the excited donor to the acceptor across strong hydrogen bridges. Directed energy transfer in these systems profits from the thermodynamic driving force imminent in the relaxation of an electron from a higher-energy orbital at the excited donor to the lower-lying LUMO localized at the acceptor site. Recent work on the *N*-4,6-dioxo-1,4,5,6-tetrahydropyrimidin-2-yl-*N*′-ferrocenylurea dimer (Chart 1, R′ = ferrocenyl) indicated efficient electron transfer across strong hydrogen bonds in a degenerate mixed-valent state, i.e. as a self-exchange without a thermodynamic driving force.[23] In CH_2Cl_2 the mixed-valent Fc/Fc^+ congener of the latter compound reportedly displays an intense narrow intervalence charge-transfer band in the near-infrared (NIR) as it is characteristic of a borderline Class II/III system according to the Robin and Day classification scheme.[24]

Styryl ruthenium complexes $(PhCH{=}CH)Ru(CO)Cl(PR_3)_2$ (R = Ph, ^{i}Pr) undergo one-electron oxidation at a potential of 0.33 V (R = Ph) or 0.28 V (R = ^{i}Pr, measured against the ferrocene/ferrocenium couple) that is dominated by the styryl ligand.[25] The unpaired spin of the associated radical cation is delocalized over the styryl entity with minor contributions of ∼25−30% from the $Ru(PR_3)_2$ moieties. The total spin density on the phenyl substituent of oxidized ruthenium styryl complexes (∼30%) clearly surpasses that on a cyclopentadienyl ligand in ferrocinium ions. We therefore mused that electronic interactions in partially oxidized mixed-valent forms of hydrogen bonded, dimeric styryl ruthenium complexes should even be stronger than those in the analogous ferrocene system. $Ru(PR_3)_2(CO)Cl$ substituted vinyl complexes have the added benefit of providing charge-sensitive IR labels by virtue of the ruthenium bonded carbonyl and vinyl ligands. The shift and pattern of the CO and vinyl vibrations upon oxidation may thus be used for mapping the efficacy and time scale of intramolecular electron transfer. These assets have successfully been employed to establish charge and spin delocalization in divinylphenylene and butadienediyl bridged diruthenium complexes.[26−28] We therefore prepared and investigated *N*-4,6-dioxo-5,5-dibutyl- and *N*-4,6-dioxo-5,5-di-(2-propenyl)-1,4,5,6-tetrahydropyrimidin-2-yl-*N*′-(4-ethynylphenyl)urea and the corresponding P^iPr_3 ligated ruthenium and osmium styryl derivatives. The results on these hydrogen-bonded, dimeric complexes are compared to those on a monomeric *N*-phenyl-*N*′-(4-ethenylphenyl)urea ruthenium derivative lacking the pyrimidinedione hydrogen-bond-accepting moiety.

Results

Tetrahydropyrimidine-Substituted (4-Ethynylphenyl)urea Derivatives and 4-Styrylurea Complexes. The styryl ruthenium and osmium complexes **2a**,**b** and **3a**,**b** with an appended quadruply hydrogen-bonding moiety were synthesized by reacting the corresponding 4-ethynylphenyl-substituted ureapyrimidinedione (Upy) with the hydride complexes $HM(CO)Cl(P^iPr_3)_2$ (M = Ru, Os) in CH_2Cl_2 according to Scheme 1. The known *N*-4,6-dioxo-5,5-dibutyl- and *N*-4,6-dioxo-5,5-di-(2-propenyl)-1,4,5,6-tetrahydropyrimidin-2-yl-*N*′-(4-ethynylphenyl)urea derivatives **1a**,**b**[19] were prepared in three steps from the respective disubstituted malonate, guanidinium hydrochloride, and 4-ethynylphenylisocyanate, which in turn was available from commercial 4-ethynylaniline and triphosgene. The identity of the compounds as the target styryl complexes was readily established by virtue of the ^{1}H NMR signals of an ABX_2-spin system of the vinyl protons at 8.6−8.2 ppm (MC*H*) and at 6.0−5.5 ppm (MCH=C*H*) with clearly resolved ^4J coupling to two equivalent phosphorus nuclei for the latter one, the typical vinyl resonances in ^{13}C NMR at ∼150 ppm ($M{-}C_\alpha$) or 135 ppm ($M{-}C_\alpha{=}C_\beta$), the singlet resonance in ^{31}P NMR of the equivalent phosphorus nuclei and the single CO band at 1910 (M = Ru) or 1895 (M = Os) cm^{-1} in the IR. Owing to the solubilizing substituents at the 5-positions of the Upy skeleton and the P^iPr_3 ligands, all complexes readily dissolve in low-polarity solvents such as chloroform, dichloromethane, THF, or mixtures of these solvents with methanol, while they are only sparingly soluble in neat methanol or hexanes.

X-ray crystallography on alkynes **1a**,**b** (Figure 1 and Figure S1 of Supporting Information) and on the ruthenium complex **2a**·$2CH_2Cl_2$ (Figure 2) revealed the expected dimeric structures

(18) Söntjens, S. H. M.; Sijbesma, R. P.; van der Genderen, M. H. P.; Meijer, E. W. *J. Am. Chem. Soc.* **2000**, *122*, 7487–7493.
(19) Baruah, P. K.; Gonnade, R.; Phalgune, U. D.; Sanjayan, G. D. *J. Org. Chem.* **2005**, *70*, 6461–6467.
(20) Zhang, J.; Hoeben, F. J. M.; Pouderoijen, M. J.; Schenning, A. P. H. J.; Meijer, E. W.; De Schryver, F. C.; De Feyter, S. *Chem. Eur. J.* **2006**, *12*, 9046–9055.
(21) Sánchez, L; Sierra, M; Martín, N.; Myles, A. J.; Dale, T. J.; Rebek, J., Jr.; Seitz, W.; Guldi, D. M *Angew. Chem.* **2006**, *118*, 4753–4757.
(22) Segura, M. L; Sánchez de Mendoza, J; Martín, N.; Guldi, D. M. *J. Am. Chem. Soc.* **2003**, *125*, 15093–15100.
(23) Sun, H.; Steeb, J.; Kaifer, A. E. *J. Am. Chem. Soc.* **2006**, *128*, 2820–2821.
(24) Robin, M. B.; Day, P. *Adv. Inorg. Chem. Radiochem.* **1967**, *10*, 247–422.
(25) Maurer, J; Linseis, M; Sarkar, B.; Schwerderski, B.; Niemeyer, M.; Kaim, W.; Záliš, S; Anson, C.; Zabel, M.; Winter, R. F. *J. Am. Chem. Soc.* **2008**, *130*, 259–268.
(26) Maurer, J.; Sarkar, B.; Kaim, W.; Winter, R. F.; Záliš, S. *Chem.-Eur. J.* **2007**, *13*, 10257–10272.
(27) Maurer, J.; Sarkar, B.; Schwederski, B.; Kaim, W.; Winter, R. F.; Záliš, S. *Organometallics* **2006**, *25*, 3701–3712.
(28) Maurer, J.; Sarkar, B.; Zalis, S.; Winter, R. F. *J. Solid State Electrochem.* **2005**, *9*, 738–749.

Scheme 1. Synthesis of the Hydrogen-Bonded Styryl Metal Complexes **2a**,**b** and **3a**,**b**

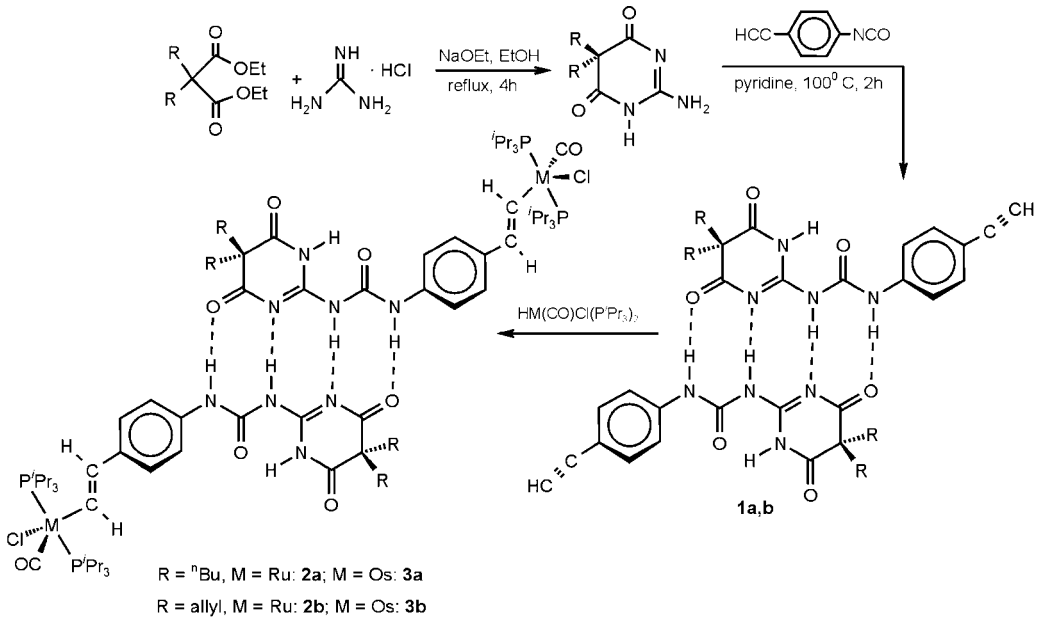

in the solid state. The centrosymmetric dimers are held together by four hydrogen bonds. Each NH proton of the urea function acts as a hydrogen-bond donor to either one imine nitrogen (pyrimidinedione-substituted NH) or one carbonyl oxygen atom (styryl-substituted NH) of the pyrimidinedione ring of another molecule. Intradimer *N*H···*N*=C distances of 3.111 Å in **1a**, 3.020 (molecule A) or 3.094 Å (molecule B) of **1b** and 3.124 Å in **2a** are flanked by shorter *N*H···*O*=C distances of 2.850 Å in **1a**, 2.823 or 2.854 Å in **1b** and 2.863 Å in **2a**. Strong hydrogen bonds of 2.598 Å in **1a**, 2.542 or 2.551 Å in **1b** and 2.550 Å in **2a** between the remaining amide of the pyrimidinedione and the urea carbonyl of the same molecule are also observed. The rigid H-bonded scaffold fixes the ruthenium−ruthenium end-to-end distance within dimeric **2a** to 24.56 Å. Intramolecular and intradimer hydrogen-bridging motifs of **1a,b** and **2a** are identical to those in *N*-alkyl-substituted 4,6-dioxo-5,5-dialkyl- and -5,5-dibenzyl-1,4,5,6-tetrahydropyrimidineurea derivatives. Intermolecular distances between the individual molecules of each dimer, however, tend to be somewhat longer as in aliphatic derivatives, where *d*(*N*H···*N*=C) and *d*(*N*H···*O*=C) values range from 2.921 to 3.030 Å and from 2.746 to 2.877 Å, respectively.[19]

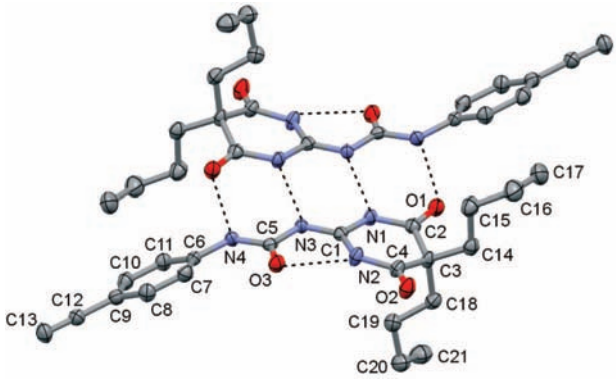

Figure 1. ORTEP plot of a dimer of alkyne **1a** with ellipsoids set at a 50% probability level. Hydrogen atoms are omitted; intra- and intermolecular hydrogen bonds are indicated as dotted lines.

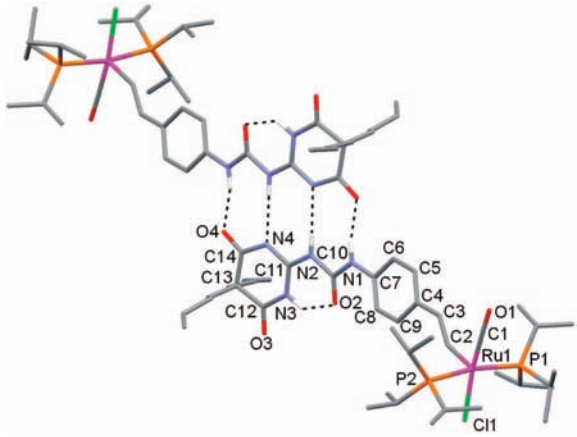

Figure 2. Capped sticks drawing of a dimer of complex **2a**. Intra- and intermolecular hydrogen bonds are indicated as dotted lines. Hydrogen atoms except for those involved in hydrogen bonding have been omitted for clarity.

Of particular note are the interplanar angles between the 4-ethynylphenyl or the styryl ruthenium planes and that of the pyrimidinedione ring of 38.8° (**1a**), 14.4° or 9.5° (**1b**), or 18.9° (**2a**), respectively. A nearly coplanar arrangement of the styryl ruthenium entity, the urea function, and the pyrimidinedione ring of **2a** is a conformational prerequisite for communicating electronic information between the ruthenium styryl and the hydrogen-bonding moieties. Torsion angles Ru−C2−C3−C4 of 172.9(7)°, C2−C3−C4−C5 of −168.1(9)° and C2−C3−C4−C9 of 13.3(14)° further attest to π-conjugation within the ruthenium styryl moiety. The square pyramidal coordination of the metal atom and bonding parameters such as the Ru−C2 (1.985(8) Å), C2−C3 (1.325(12) Å), C3−C4 (1.487(11) Å), and Ru−P bond lengths of 2.394(2) Å and 2.396(2) Å as well as the P1−Ru−P2 and Cl1−Ru−C1 bond angles of 169.58(8)° and 171.8(3)°, respectively, are in the common range of five-coordinated ruthenium vinyl, alkyl, aryl, or hydride complexes and require no further comment.[29−34] Torsion angles Cl1−Ru−C2−C3 of 175.9(9)° and C1−Ru−C2−C3 of −4.9(10)° signal that the vinyl ligand resides in the Cl1−Ru−C1 plane. The ruthenium vinyl group bisects the P1−Ru−P2 vector and forms a

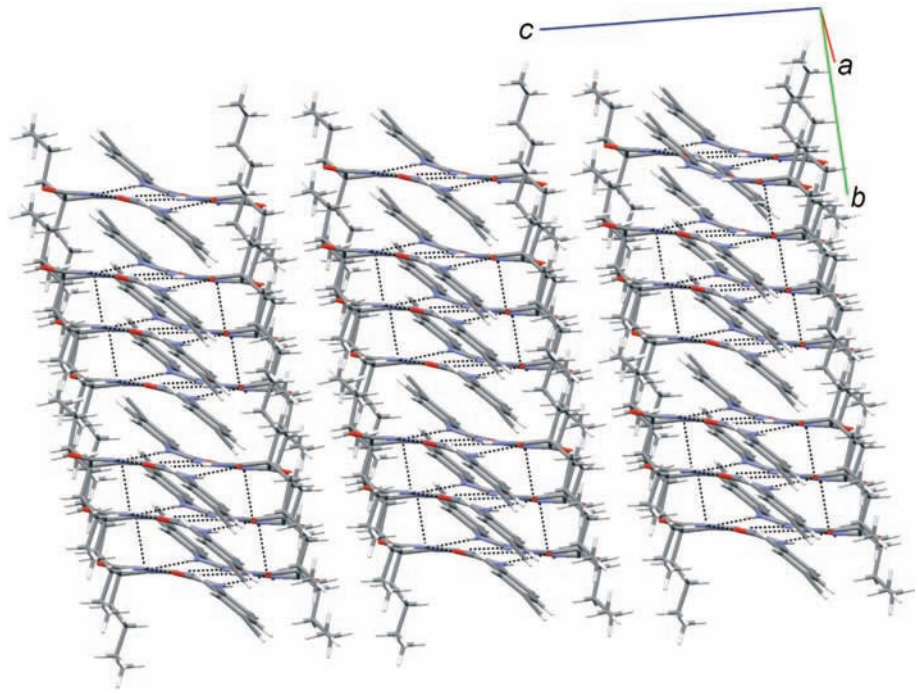

Figure 3. Packing of alkyne **1a** in the crystal. Hydrogen bonds within and between individual dimers are indicated as dotted lines.

P2−Ru−C2−C3 angle of 90.1(9)° and a P1−Ru−C2−C3 angle of 94.4(9)° as it is routinely observed for such complexes.

Compounds **1a**,**b** and **2a·2CH$_2$Cl$_2$** also show interesting packing motifs in the crystal. Common is the further association of dimers into infinite chains via *N*H···*O*=C hydrogen bridges of 3.142 Å (**1a**), 2.972 Å (**1b**), or 3.076 Å (**2a**) between the pyrimidinedione amide N2 (**1a**), N7 of molecule B in **1b** or N3 (**2a**), and the pyrimidinedione carbonyl O2 of **1a**, O2 of molecule A in **1b**, or O3 of **2a** (see Figures 3 and 4 and Figures S2 and S3 of the Supporting Information). These interdimer contacts always involve the imine nitrogen that already forms an intramolecular hydrogen bond to the urea carbonyl and the "backside" pyrimidinedione carbonyl that is not engaged in dimer formation. In **1a**, staircase-like chains of interconnected dimers run parallel to the *ab* plane, whereas in **1b** a wavy arrangement of individual dimers along the chain propagation axis is observed. Interconnected dimers within the chains are tilted by about 30° with respect to each other. In **2a·2CH$_2$Cl$_2$**, staircase-like chains of parallel disposed dimers intersect at an angle of 43.5°. Additional Ru−Cl···H$_2$CCl$_2$···HCCl$_2$H···Cl−Ru and Ru−Cl···H$_2$CCl$_2$···HCCl$_2$H···O≡C−Ru contacts interlink different chains. Each Ru−Cl ligand hydrogen bonds to one CH of each of the crystallographically distinct CH$_2$Cl$_2$ molecules with CH···Cl distances of 2.562 Å (CH$_2$Cl$_2$(1)) or 2.614 Å (CH$_2$Cl$_2$(2)). The second hydrogen atom of CH$_2$Cl$_2$(1) interacts weakly with the oxygen atom of the carbonyl ligand (C−H···O = 2.50 Å),

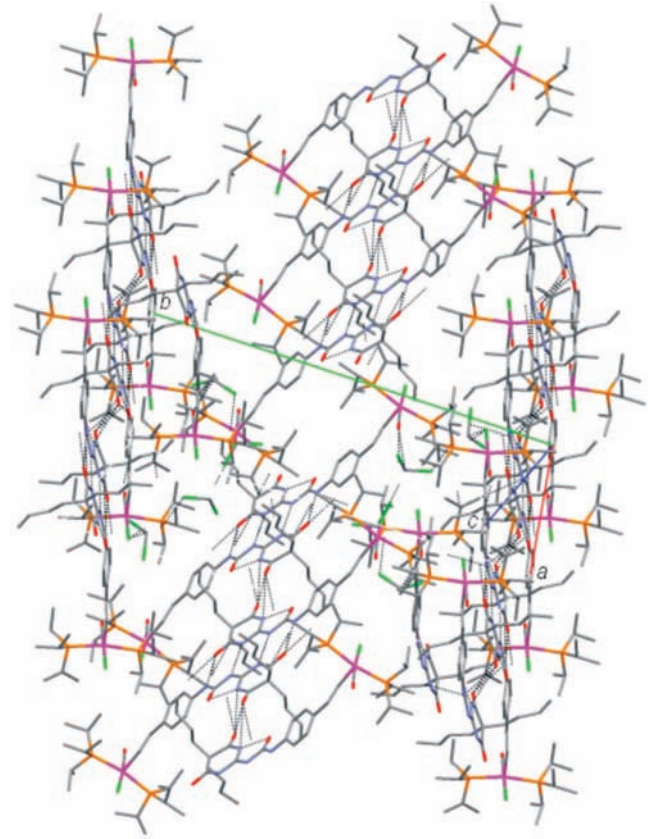

Figure 4. Packing of complex **2a·2CH$_2$Cl$_2$** in the crystal. Intra- and intermolecular hydrogen bonds are indicated as dotted lines. Hydrogen atoms have been omitted for clarity.

while the second hydrogen atom of CH$_2$Cl$_2$(2) forms a CH···Cl contact of 2.77 Å with atom Cl2 on CH$_2$Cl$_2$(1) (see Figure S4 of the Supporting Information).

(29) Maurer, J.; Linseis, M.; Sarkar, B.; Schwederski, B.; Niemeyer, M.; Kaim, W.; Záliš, S.; Anson, C.; Zabel, M; Winter, R. F. *J. Am. Chem. Soc.* **2009**, *131*, 259–268.
(30) Werner, H.; Esteruelas, M. A.; Otto, H. *Organometallics* **1986**, *5*, 2295.
(31) Huang, D.; Streib, W. E.; Bollinger, J. C.; Caulton, K. G.; Winter, R. F.; Scheiring, T. *J. Am. Chem. Soc.* **1999**, *121*, 8087–8097.
(32) Jung, S.; Ilg, K.; Brandt, C. D.; Wolf, J.; Werner, H. *Eur. J. Inorg. Chem.* **2004**, *46*, 9–480.
(33) Alcock, N. W.; Cartwright, J.; Hill, A. F.; Marcellin, M.; Rawles, H. M. *J. Chem. Soc., Chem. Commun.* **1995**, 369–370.
(34) Maruyama, Y.; Yamamura, K.; Sagawa, T.; Katayama, H.; Ozawa, F. *Organometallics* **2000**, *19*, 1308–1318.

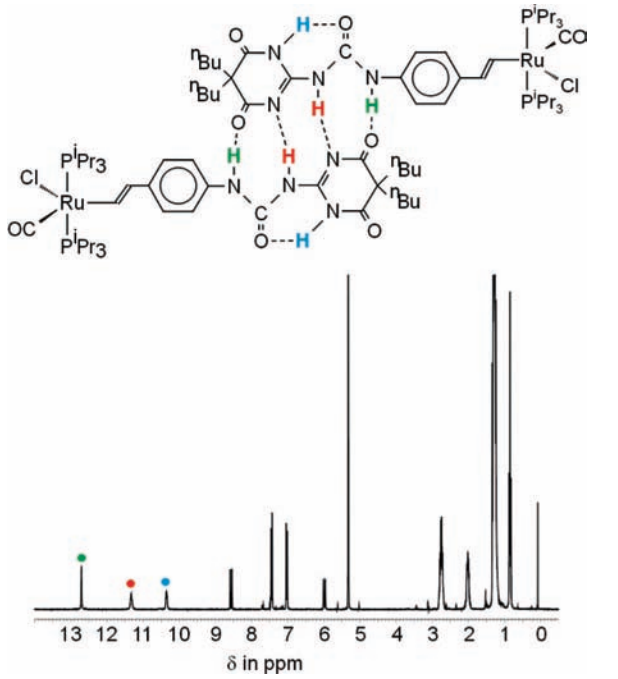

Figure 5. ^{1}H NMR spectrum of complex **2a** in CD_2Cl_2 (293 K, c = 1.1 mol/L). Hydrogen atoms involved in hydrogen bonding are marked; the color coding corresponds to that in the chart at the top.

^{1}H NMR spectroscopy shows by virtue of the characteristic low-field shifts of the urea and imine hydrogen atoms engaged in the intramolecular and intradimer hydrogen bonding that the dimeric structures of the parent alkyne and its derived ruthenium and osmium vinyl complexes are maintained in CD_2Cl_2 and $CDCl_3$ solutions.[12] Proton signals in the respective spectral region were assigned by HMBC and HSQC measurements, which give δ (NH···OC, intermolecular) ~12.7 ppm, NH···N (intermolecular) ~11.5 ppm, and δ (NH···OC, intramolecular) ~10.5 ppm (see Figure 5). The latter proton (blue color in Figure 5) easily exchanges with the inner urea proton (red color) and much more slowly with the outer urea proton (green color in Figure 5) as follows from these NMR experiments. The former process involves tautomerization of the urea NH and the imine N groups and rotation of the tetrahydropyrimidine ring. All these signals appear at much lower field than in nonassociated alkyl or aryl urea derivatives.[12] This is also true for CD_2Cl_2 solutions in the presence of a large excess of NBu_4PF_6 and at concentrations (1.1 mM in the complex, 0.1 M in the supporting electrolyte) as they are typically employed in voltammetry (see Figure S5 of the Supporting Information). Addition of CD_3OH to CD_2Cl_2 solutions leads to broadening and appreciable high-field shifts of the =NH signals, which accounts for the anticipated interference of that solvent with hydrogen bonding. In agreement with observations on similar systems,[35−37] ^{1}H NMR spectra of alkynes **1a**,**b** in CD_3CN display NH shifts very similar to those in $CDCl_3$ or CD_2Cl_2 which argues against interference of the weakly hydrogen-bond-donating[38−40] and moderately hydrogen-bond-accepting acetonitrile solvent[38,39] with dimerization via four hydrogen bonds. Fast solvolysis of the metal−Cl bond of complexes **2a**,**b** and **3a**,**b** does not allow us to record their NMR spectra in CD_3CN solvent.

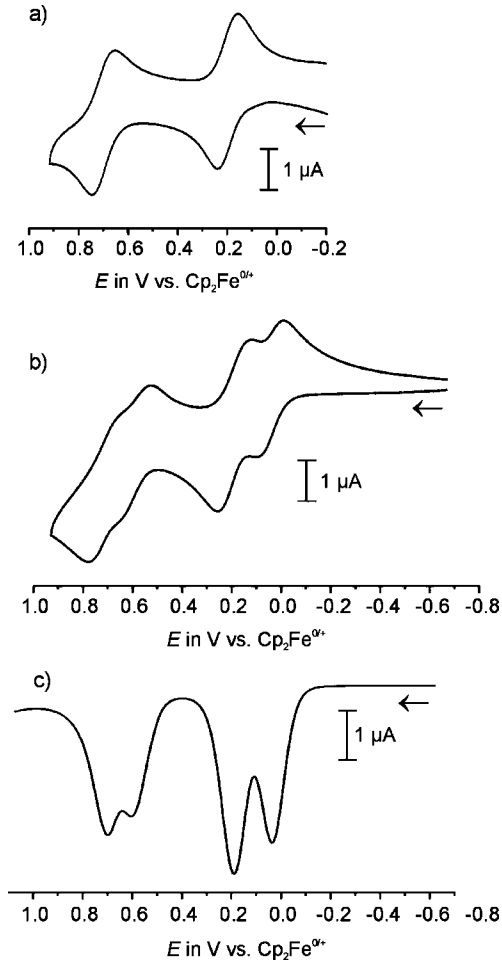

Figure 6. (a) Voltammogram of a 0.17 mM solution of complex **2a** in CH_2Cl_2/NBu_4PF_6 (0.1 M) at rt and υ = 0.1 V/s. (b) Voltammogram of a mixture of **2a** and **3b** in CH_2Cl_2/NBu_4PF_6 (0.1 M) at rt and υ = 0.1 V/s after 20 h of equilibration. (c) Square wave voltammogram of the solution as in (b) (ν = 15 Hz).

Electrochemical investigations on the hydrogen-bonded dimers of **2a**,**b** and **3a**,**b** were performed in CH_2Cl_2/0.1 M NBu_4PF_6 as the electrolyte. Each complex undergoes two consecutive oxidations. The first wave is chemically reversible, but the second one is only partially so with reversibility coefficients in the range of 0.76−0.90 at 0.1 V/s. Half-wave potential separations are in the range of 515−530 mV (Figure 6a). Both waves are somewhat broader as would be expected of a fast uncomplicated one-electron process as it is shown by the larger peak-to-peak separations and half-widths of the forward (anodic) peak when compared to the internal decamethylferrrocene standard. Digital simulations of the experimental voltammograms[41] are most consistent with somewhat sluggish electron-transfer kinetics (electron-transfer rates $k_{ET} \approx 0.005$ cm^{-1} and 0.0038 cm·s^{-1} for the first and second oxidation, respectively).[42] The osmium complexes **3a**,**b** are oxidized at ~175 mV lower potential than their ruthenium congeners **2a**,**b**. Redox potentials and peak-to-peak separations are listed in Table 1.

(35) Sharif, S.; Denisov, G. S.; Toney, M. D.; Limbach, H.-H. *J. Am. Chem. Soc.* **2007**, *129*, 6313–6327.
(36) Pérez, E. M.; Dryden, D. T. F.; Leigh, D. A.; Teobaldi, G.; Zerbetto, F. *J. Am. Chem. Soc.* **2004**, *126*, 12210–12211.
(37) Bohne, C.; Ihmels, H.; Waidelich, M.; Yihwa, C. *J. Am. Chem. Soc.* **2005**, *127*, 17158–17159.
(38) Marcus, Y. *Chem. Soc. Rev.* **1993**, *22*, 409–416.
(39) Abraham, M. H. *Chem. Soc. Rev.* **1993**, *22*, 73–83.
(40) Stolov, A. A.; Kamalova, D. I.; Borisover, M. D.; Solomonov, B. N.; Remizov, A. R. *Spectrochim. Acta* **1994**, *50A*, 145–150.
(41) Rudolph, M.; Feldberg, S. *DigiSim3, Version 3.03*, Bioanalytical Systems, Inc.:West Lafayette, IN, 1994.

Table 1. Data Pertinent to Electrochemical Investigations on Vinyl Complexes **2a**,**b**, **3a**,**b** and **5** at $v = 100$ mV/s

cmpd	$E_{1/2}^{0/+}$ in V	$E_{p,f} - E_{p,f/2}$/ ΔE_p in mV	$E_{1/2}^{0/+}$ in V	$E_{p,f} - E_{p,f/2}$/ ΔE_p in mV	D in 10^{-9} $m^2 \cdot s^{-1}$
2a	0.19	63/76	0.71	61/75	0.55(7)
2b	0.195	60/80	0.70	60/80	not measured
3a	0.020	68/94	0.550	104/136	not measured
3b	0.015	58/79	0.540	70/109	not measured
5	0.085	57/59	0.60	58/60	0.70(3)

The overall wave pattern is largely invariant to the addition of methanol which breaks the intermolecular hydrogen bonds as follows from ^{1}H NMR spectroscopy. The only effects were the partial loss of chemical reversibility, broadening of particularly the second wave and its final disappearance into the solvent background when more methanol was added (Figure S6 of the Supporting Information). This contrasts to observations by Kaifer et al. on the related ferrocenyl system where the two waves in CH_2Cl_2/NBu_4PF_6 evolved into a single one upon addition of even the weakly hydrogen-bonding acetonitrile.[23] Addition of the osmium complex **3b** to the ruthenium complex **2a** results in rapid scrambling and the formation of a mixture of dimers $(\mathbf{2a})_2$, **2a/3b** and $(\mathbf{3b})_2$ as was ascertained by ^{1}H NMR spectroscopy. At $T = 203$ K scrambling is sufficiently slow so that a separate set of resonance signals can be observed for the mixed **2a/3b** dimer (see Figure S7 of the Supporting Information). Such solutions still showed only the two separated pairs of waves (cyclic voltammetry) or peaks (square wave voltammetry) at the same potentials as the pure complexes $(\mathbf{2a})_2$ and $(\mathbf{3b})_2$ (Figure 6b,c) but neither a new pair of waves/peaks nor a potential shift that might be expected of a mixed dimer **2a/3b** if the two subunits were interacting.

Comparison of the slopes from i vs $t^{1/2}$ plots in chronoamperometry and of the step heights in steady-state voltammetry to those of the decamethylferrocene standard according to the method of Baranski[43] finally established that each voltammetric wave of complexes **2a**,**b** and **3a**,**b** involves the loss of *two electrons* per ruthenium or osmium dimer. In addition, combined chronocoulometry (CC) and linear sweep voltammetry (LSV) data on $(\mathbf{2a})_2$ and $(\mathbf{3a})_2$ are only consistent with the transfer of one electron for every styryl ruthenium subunit. Assuming that each wave involves the transfer of one electron per dimer would give the unrealistic result that these complexes have a diffusion coefficient similar to that of ferrocene. Furthermore, diffusion coefficients determined by CC and LSV would differ by a factor of 2. We therefore conclude that the Upy-bridged dimeric styryl complexes do not exhibit any electrochemically detectable electronic coupling between the individual styryl metal subunits.

Wave splittings in electrochemical measurements are one first indicator, but are not wholly conclusive for the efficacy of electronic coupling between bridged redox sites in mixed-valent systems.[28,44,45] We therefore utilized the oxidation-state sensitive spectroscopic tags of the complexes **2a**,**b** and **3a**,**b** to independently probe for such interactions and for charge delocalization. When the first oxidation of hydrogen-bonded dimers $(\mathbf{2a})_2$ and $(\mathbf{2b})_2$ was followed inside an optically transparent thin-layer electrolysis cell, the single band of the metal−carbonyl stretch shifted from 1912 to 1967 cm^{-1} without any detectable intermediate (Table 3, Figure 7, and Figure S8 of the Supporting Information). The Ru−CO band shift upon oxidation is a highly sensitive measure of the loss of electron density from the metal. As the electron density at the metal atom decreases, metal backdonation into the CO π^* orbitals is weakened. This in turn strengthens the CO bond and shifts the CO band to higher energy. Redox couples $Ru(PR_3)_2(CO)_3^{0/+}$ display oxidation-induced CO band shifts of about 120−130 cm^{-1} and provide benchmark systems for the effects of a largely metal-centered oxidation in ruthenium chemistry.[46] Large styryl ligand contributions of about 70% to the HOMO in the complex $(CO)Cl(P^iPr_3)_2Ru(CH{=}CHPh)$ lead to an appreciably smaller CO band shift of 65 cm^{-1} upon one-electron oxidation.[29] The 55 cm^{-1} shift observed for complexes **2a**,**b** closely resembles this value, but signals an even larger ligand contribution in the urea-substituted system. The somewhat lower CO band shift compared to the unsubstituted styryl complex is readily explained by the electron-donating property of the urea substituent at the para position which further aids in charge delocalization. The osmium complexes **3a**,**b** show slightly lower absolute $\tilde{\nu}$(CO) shifts but give otherwise identical results (Table 3).

Other IR spectroscopic effects include slight red-shifts of the multiple NH bands that originate from the hydrogen-bonded imine groups and intensity changes but hardly any shift of the associated higher-energy urea and pyrimidinedione carbonyl bands (see Figures 7 and Figures S8 and S9 of the Supporting Information). Stronger changes in the region below 1600 cm^{-1} cannot unambiguously be assigned due to the close proximity of the CNH stretching and bending modes with the C=C stretch of the ruthenium styryl moiety. Vibrational data in various oxidation states and tentative assignments based on literature values for pyrimidine-4,6-diones,[47] ureas,[48] and styryl complexes[27,29] and on our quantum chemical calculations (*vide infra*) are collected in Tables 2, 3, and 5.

The effects of the second oxidation were exemplarily studied with complex **2b**. The most notable feature is the further blue-shift of the Ru−CO band to 1990 cm^{-1} (Table 3). The small CO band shift of only 23 cm^{-1} signals that the second oxidation is also dominated by the styryl ligand with an even smaller contribution of the metal atom. This parallels our results on pyrenylvinyl complexes $(PR_3)_2(L)(CO)ClRu(CH{=}CH\text{-}2\text{-}pyrenyl)$ (R = ^{i}Pr, L = none; R = Ph, L = isonicotinate).[25]

The neutral complexes **2a**,**b** and **3a**,**b** feature intense electronic bands at ~265, 297, and 360 nm that are assigned to intraligand $\pi \rightarrow \pi^*$ and ligand-to-metal charge-transfer (LMCT) or mixed intraligand and metal-to-ligand charge transfer (ILCT)/MLCT absorptions (see Table S7 and Figure S16 of the Supporting Information), respectively, and a weak band near 520 nm due to a forbidden transition within the d-manifold that is characteristic of d^6 ML_5 complexes.[49,50] This pattern is very similar to that of related styryl complexes and thus seems unperturbed by hydrogen bonding. UV/vis/NIR spectroelectro-

(42) The alternative model of two closely spaced one-electron waves is only compatible with a splitting of less than 35 mV between the 0/+ and +/2+ waves and gives a less accurate fit.
(43) Baranski, A. S.; Fawcett, W. R.; Gilbert, C. M. *Anal. Chem.* **1985**, *57*, 166–170.
(44) Barrière, F.; Geiger, W. E. *J. Am. Chem. Soc.* **2006**, *128*, 3980–3989.
(45) Glöckle, M.; Kaim, W.; Fiedler, J. *Organometallics* **1998**, *17*, 4923–4925.
(46) Sherlock, S. J.; Boyd, D. C.; Moasser, B.; Gladfelter, W. L. *Inorg. Chem.* **1991**, *20*, 3626–3632.
(47) Ahluwalia, V. K.; Sharma, S.; Kaur, M. *Spectrochim. Acta* **1989**, *45A*, 917–927.
(48) Lin-Vien, D.; Colthup, N. B.; Fateley, W. G.; Grasselli, J. G. *The Handbook of Infrared and Raman Characteristic Frequencies of Organic Molecules*; Academic Press: San Diego, 1991.
(49) Bressan, M.; Rigo, P. *Inorg. Chem.* **1975**, *14*, 2286–2288.
(50) Briggs, J. C.; McAuliffe, C. A.; Dyer, G. *J. Chem. Soc., Dalton Trans.* **1984**, 423–427.

Table 3. IR Spectra of **2a**,**b**, and **3b** in the Neutral and the Monooxidized State and of $\mathbf{2b}^{2+}$ ($\tilde{\nu}$ in cm^{-1})

	2a	$2a^+$	**2b**	$2b^+$	$\mathbf{2b}^{2+}$	**3b**	$3b^+$
ν (NH)	3412, 3289, 3260, 3179, 3100	3380, 3276, 3230, 3184, 3152, 3096	3397, 3288, 3180	3378, 3284, 3193, 3147	3384, 3319, 3201		
ν (CO)	1912	1967	1912	1967	1990	1894	1945
ν $(CO)_{pmd,\ as}$	1733	1738	1737	1740	1754	1737	1740
ν $(CO)_{pmd,\ as}$ + δ $(CNH)_{urea}$	1703	1703	1706	1706	1742	1707	1705
ν $(CO)_{pmd,\ as}$	1667	1668	1663	1667	1651	1660	1665
+ δ $(CNH)_{urea}$	1648	1648	1650, 1643	1649, 1643	1641		
δ $(CNH)_{urea}$ + δ $(CNH)_{pmd}$ [+δ $(C{=}C)_{styryl}$]	1585, 1560	1564	1588, 1565	1598, 1561	1603, 1577	1597, 1557	1570
δ $(CNH)_{urea}$ + δ $(CNH)_{pmd}$	1525, 1507, 1483	1513, 1483	1509, 1483, 1471	1525, 1507, 1483, 1471	1528	1508	1512

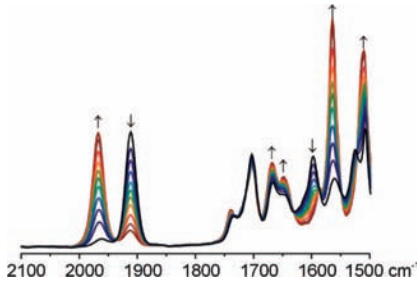

Figure 7. IR spectroelectrochemistry on complex **2a** (DCE/NBu_4PF_6, rt) in the carbonyl, C=N and C=C regions. Spectroscopic changes during the first oxidation.

Table 2. IR Spectra of Alkynes **1a**,**b** and **4** and of Complex **5** ($\tilde{\nu}$ in cm^{-1}) in the Neutral and the Monooxidized State and Calculated Data for the $\mathbf{Upy^{Me}}$ Monomer and Dimeric $(\mathbf{Upy^{Me}})_2$[a]

	1a	**1b**	**4**	**5**	$\mathbf{5}^+$	$(\mathbf{Upy^{Me}})_2$	$\mathbf{Upy^{Me}}$
ν (CO)	–	–	–	1910	1964	–	–
ν (≡CH),	3300	3290	3290	–	–	–	–
ν (C≡C)	2107	2105	2106				
ν $(CO)_{pmd,\ as}$	1735	1734	–	–	–	1747	1748
ν $(CO)_{pmd,\ as}$ + δ $(CNH)_{urea}$	1703	1702	–	1722	1722	1715	1715
ν $(CO)_{pmd,\ as}$ + δ $(CNH)_{urea}$	1671	1665	1635			1658	1707
δ $(CNH)_{urea}$	1592	1592	1587	1591	1581	1613	1603
+ δ $(CNH)_{pmd}$ [+δ $(C{=}C)_{styryl}$]			1559	1562	1572	1568	1531
δ $(CNH)_{urea}$	1528	1528	1505		1514	1527	1495
+ δ $(CNH)_{pmd}$	1509	1508					

[a] DFT/B3LYP calculated energies are scaled by the factor 0.957.

chemistry revealed the appearance of a split absorption near 430 nm and a lower-energy absorption band peaking at ~700 nm upon the first oxidation (Figure 8). Such bands are routinely observed for the radical cations of styryl ruthenium complexes and involve a $\pi \rightarrow \pi^*$ transition within the oxidized metal styryl chromophore (βHOMO → βLUMO, calculated energy 1.81 eV, λ = 684 nm) and nearly degenerate ILCT and metal-to-ligand charge transfer (MLCT) transitions (αHOMO→αLUMO+1 and βHOMO−8→βLUMO, calculated energies 3.04 and 3.05 eV, λ = 408 and 406 nm) as well as a close-lying strongly mixed transition calculated at 3.14 eV (395 nm, see Table S8 and Figure S17 of the Supporting Information).

Partial in situ oxidation of a solution of complex **2a** inside an ESR tube provided a solution that was ESR silent in fluid solution but revealed a weak signal in a frozen matrix at 110 K at g = 2.033 which again is in the typical range of styryl ruthenium radical cations.

The Urea-Substituted Styryl Complex 5. It is now of interest to compare the strongly hydrogen-bonded complexes **2a**,**b** and **3a**,**b** with similarly substituted styryl complexes that will not dimerize in solution. To these ends we prepared *N*-phenyl-*N*′(4-ethynylphenyl)urea (**4**, Chart 2) and converted it to the ruthenium vinyl complex **5**. ^{1}H NMR spectroscopy showed the NH proton signals of the urea moiety at ~7 ppm and thus at considerably higher field than in the dimers of **2a**,**b** and **3a**,**b**.

X-ray crystallographic investigations on alkyne **4** and complex **5** disclosed association through hydrogen bonding involving the urea functions in crystalline **4**, but not in complex **5**. Hydrogen bridges between the NH protons and the urea carbonyl assemble individual molecules of alkyne **4** into one-dimensional infinite chains that run along the crystallographic *a* axis (Figure 9). *N*H···*O*=C distances between the two crystallographically independent molecules of **4** range from 2.856 to 2.885 Å. The aryl rings of each molecule are almost perpendicular to each other with angles of 87.6° or 88.4° between their best planes. CH···C=C_{arene} interactions H5··C1 (2.869 Å), H5···C2 (2.750 Å), H25···C21 (2.876 Å), H25···C22 (2.763 Å) and CH···C_{arene} interactions H8···C11 (2.891 Å), H11···C8 (2.849 Å), H29···C32 (2.853 Å), H32···C29 (2.879 Å) between perpendicular arene rings interconnect these chains to infinite stacks. These stacks are arranged in an antiparallel fashion. Individual molecules belonging to different stacks tilt at an angle of about 59° or 122° with respect to the crystallographic *b* axis. This generates a fishbone pattern that propagates along the *c* axis (Figure S11 of the Supporting Information). The alkynyl groups of a stack point in the same direction and toward those of a neighboring stack. This allows for additional weak contacts between the acetylenic hydrogen atom H35 and alkyne carbon atoms C14 and C15 of 2.966 or 2.964 Å.

In complex **5**, none of these interactions is preserved. Rather, hydrogen bonds between the chloride ligand and both NH functions of the immediate neighbor molecule with *N*H···*Cl* distances of 2.53 Å and 2.76 Å for two molecules A or 2.42 Å and 2.72 Å for two molecules B lead to an alternative mode of association into weakly bonded dimers (Figure 10). These hydrogen-bonding interactions are very likely not maintained in solution as follows from the NH proton shifts. In the crystal, dimers of molecules A and B form a criss-cross pattern parallel to the *ac* plane and are only weakly connected by H···O contacts of 2.54 Å between the carbonyl ligand and H(23) of the styryl ligand (see Figure S12 of the Supporting Information).

Individual molecules A and B of **5** have similar metrical parameters in the vicinity of the metal atom but differ somewhat with respect to the styryl urea moiety. The most notable differences pertain to the vinyl group where the short−long alternation of molecule A with C=C and =C−C bond lengths of 1.246(13) Å and 1.496(17) Å, respectively, is more pronounced than for molecule B (1.302(11) Å and 1.429(15) Å),

Table 5. DFT/B3LYP Calculated Vibration Energies ($\tilde{\nu}$ in cm^{-1}) for $\mathbf{2^{Me}}$, $\mathbf{3^{Me}}$, and $\mathbf{5^{Me}}$ Model Complexes in the Neutral and Oxidized States[a]

	2^{Me}	$2^{Me\,\bullet+}$	$2^{Me\,2+}$	3^{Me}	$3^{Me\,\bullet+}$	5^{Me}	$5^{Me\,\bullet+}$
ν (CO)	1912	1956	1993	1900	1943	1911	1952
ν $(CO)_{pmd,\ as}$	1767	1777	1792	1767	1776	–	
ν $(CO)_{pmd,\ as}$ + δ $(CNH)_{urea}$	1751	1762	1768	1751	1762	–	
ν $(CO)_{pmd,\ as}$ + δ $(CNH)_{urea}$	1720	1732	1723	1720	1732	1719	1737
δ $(CNH)_{urea}$ + δ $(CNH)_{pmd}$ [+δ $(C{=}C)_{styryl}$]	1610	1618	1614	1609	1618	1571	1592
	1567	1585		1569	1584	1555	1584
δ $(CNH)_{urea}$ + δ $(CNH)_{pmd}$	1500	1535	1599	1500	1536	1500	1510
	1467	1464	1464	1467	1465	1480	1492

[a] Calculated frequencies are scaled by the factor 0.957.

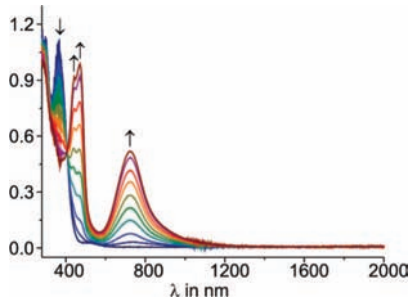

Figure 8. UV/vis/NIR spectroelectrochemistry on complex **2b** (DCE/NBu_4PF_6, rt). Spectroscopic changes during the first oxidation.

Chart 2. Phenylureyl-Substituted Alkyne **4** and Styryl Complex **5**

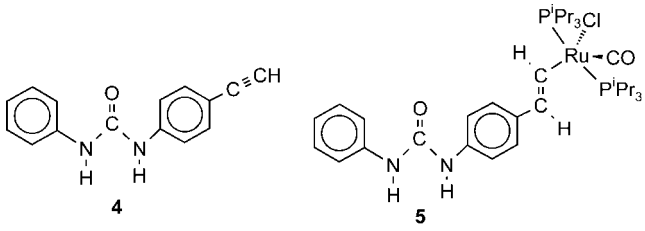

and to the vicinity of the urea carbonyl C atom, which shows more dissimilar OC−N bond lengths of 1.329(15) Å and 1.433(13) Å for molecule B than for molecule A, where values of 1.365(15) Å and 1.392(12) Å are found. The longer C−N bond always involves the styryl-bonded nitrogen atom. The C=C double bond, particularly of molecule A, is unrealistically short, and the =C−C bond is too long. This points to cocrystallization of two (or more) conformers that differ by rotation around the Ru−C vinyl bond.[51] All our attempts to resolve this apparent disorder were, however, unsuccessful. The plane of the styryl ligand is roughly coplanar to the urea function with a tilt angle of 5.3° for molecule A and 8.2° for molecule B. This contrasts to a 29.1° (molecule A) or 28.6° (molecule B) tilt angle between the terminal phenyl ring and the urea plane. Common to both molecules is a considerably larger quinoidal distortion[52] of the coplanar styryl unit than of the other phenyl ring. Thus, the opposing CH−CH bond lengths of the phenylene substituent are about 8 pm longer than the flanking ones, whereas this difference is reduced to about 3 pm for the monosubstituted phenyl ring at the other terminus. This provides more evidence for efficient conjugation between the styryl ruthenium and the urea functions in these complexes.

Voltammetry on complex **5** showed two consecutive one-electron oxidations with a half-wave potential separation similar to but half-wave potentials ~105 mV lower than those of complexes **2a**,**b** (Figure 11). This sizable cathodic shift upon replacement of the electron-withdrawing 4,6-dioxo-1,4,5,6-tetrahydropyrimidin-2-yl entity by a phenyl group is an indication of at least some electronic conjugation across the entire styryl urea moiety. IR-spectra recorded during the first oxidation revealed a blue-shift of the Ru−CO band of 54 cm^{-1} upon the first oxidation which is identical to those observed for the **2a**,**b** and **3a**,**b** dimers within the error margins (Figure 12). Due to the absence of the 4,6-dioxo-1,4,5,6-tetrahydropyridinyl substituent, the spectral pattern in the 1750−1500 cm^{-1} range is much simpler and again reveals hardly any shift of the urea carbonyl and CNH bands upon oxidation. There is likewise only a small red-shift of the NH bands from 3423 and 3400 cm^{-1} to 3415 and 3384 cm^{-1} (see Figure S13 of Supporting Information). Just like the *N*-4,6-dioxo-1,4,5,6-tetrahydropyrimidin-2-yl-*N*′(4-ethenylphenyl) (styryl Upy) ruthenium complexes **2a**,**b**, **5** displays intense $\pi\rightarrow\pi^*$ and LMCT charge-transfer absorptions at 312 and 337 nm and, at 510 nm, the weak absorption of a square pyramidal Ru(II) ML_5 system. During stepwise oxidation, rather intense absorption bands at ~450 nm and at 766 nm appear (Figure 13). The red-shift of the low-energy band of $\mathbf{5}^{\bullet+}$ when compared to $(\mathbf{2a}^{\bullet})_2^{2+}$ relates to the lower electron-accepting/stronger electron-donating properties of the urea substituent compared to those of the Upy one which destabilizes the corresponding donor orbital(s) below the SOMO.

Quantum Chemistry. Quantum chemical studies were performed in order to better understand the behavior of the dimeric Upy complexes and, in particular, to rationalize the absence of any detectable electronic coupling between individual monomers across the strong quadruple hydrogen bond. The calculations were performed on simplified models of monomers $\mathbf{Upy^{Me}}$, $\mathbf{2^{Me}}$, $\mathbf{3^{Me}}$, and $\mathbf{5^{Me}}$ and dimers $(\mathbf{Upy^{Me}})_2$ (see Figure S14, Supporting Information) and $(\mathbf{2^{Me}})_2$ with PMe_3 instead of P^{i}Pr$_3$ ligands and methyl substituents instead of ^{n}butyl or 2-propenyl groups on the quaternary carbon of the 4,6-dioxo-1,4,5,6-tetrahydropyrimidinyl ring (Chart 3). Calculated minimum structures agree reasonably well with the experimentally observed ones (X-ray) as is evident from the comparison in Table 4 (see also Chart 4). With the exception of bond C11−N2 which connects the urea function to the pyrimidinedione ring, all other bond lengths differ by, at most, 4 pm. The quinoidal distortion of the styryl ring, however, is not accounted for by the calculations.

IR-spectroscopy of dimers $(\mathbf{2a})_2$, $(\mathbf{2b})_2$, and $(\mathbf{3b})_2$ has given multiple intense absorptions in the carbonyl, C=C and CNH regions. DFT calculations on $\mathbf{2^{Me}}$, $\mathbf{3^{Me}}$ and $\mathbf{5^{Me}}$ and their oxidation products describe the energy of the Ru−CO stretching vibration ν(CO) and its shift to higher wavenumbers upon oxidation reasonably well (Table 5). Similar to our results on other vinyl ruthenium complexes[25,27] the shift of ν(CO) upon the first oxidation is underestimated which

(51) Hall, M. B.; Niu, S.; Reibenspies, J. H. *Polyhedron* **1999**, *18*, 1717–1724.
(52) Rathore, R.; Lindeman, S. V.; Kumar, A. S.; Kochi, J. K. *J. Am. Chem. Soc.* **1998**, *120*, 6931–6939.

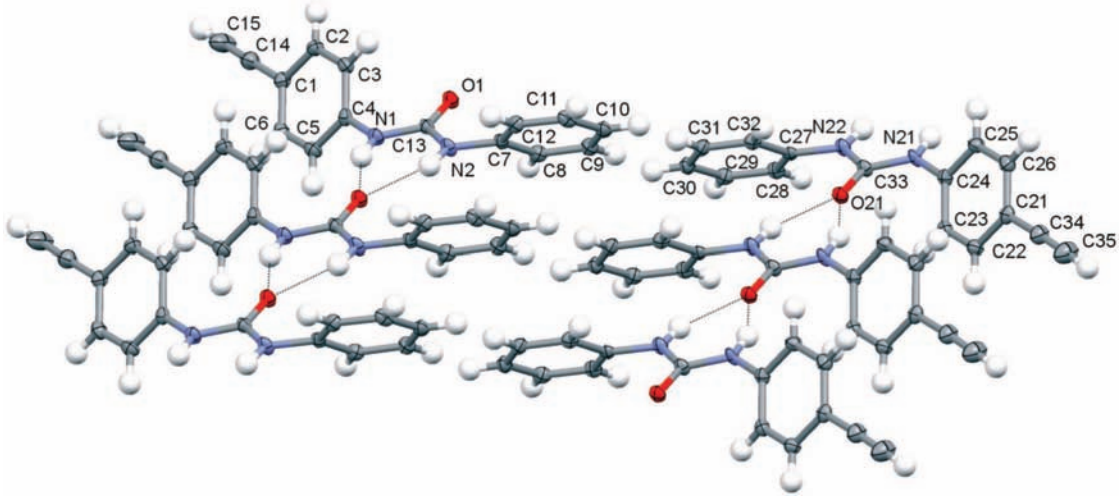

Figure 9. ORTEP plot of the chains of hydrogen-bonded molecules of alkyne **4** with ellipsoids set at a 50% probability level. Intermolecular hydrogen bonds are indicated as dotted lines.

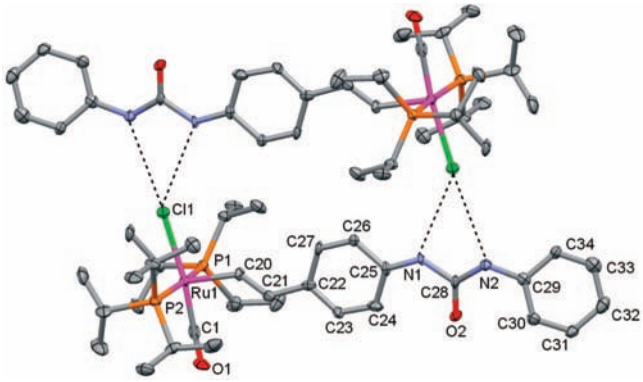

Figure 10. ORTEP plot of a weakly associated dimer of two molecules A of complex **5** with ellipsoids set at a 50% probability level. Hydrogen atoms are omitted for clarity; intermolecular hydrogen bonds are indicated as dotted lines.

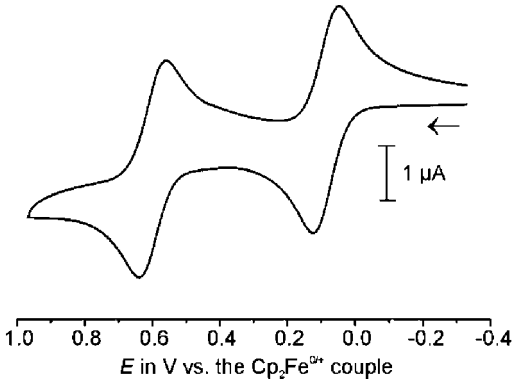

Figure 11. Voltammogram of a 0.23 mM solution of complex **5** in CH_2Cl_2 /NBu_4PF_6 (0.1 M) at rt and $\upsilon = 0.1$ V/s.

points to an overestimated contribution of the modified styryl ligand to the redox orbital. We felt that a more detailed analysis of these bands and their evolution upon oxidation might provide a tool to experimentally map the extent to which the developing positive charges are delocalized into the crucial hydrogen-bonding segment of these molecules. In order to aid the assignment of the multiple absorptions in that region we calculated the stretching frequencies of the *N*-4,6-dioxo-5,5-dimethyl-1,4,5,6-tetrahydropyrimidin-2-yl-

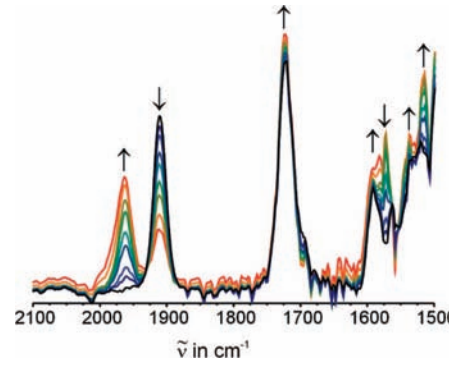

Figure 12. IR spectroelectrochemistry on complex **5** (DCE/NBu_4PF_6, rt) in the carbonyl, *C*=N and C=C regions.

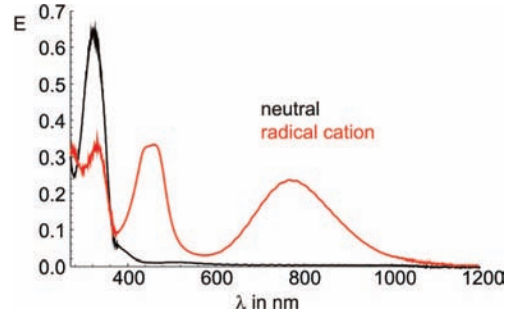

Figure 13. UV/vis/NIR spectra of complex **5** (black trace) and of $[\mathbf{5}]^{\bullet+}$ (red trace) in (DCE/NBu_4PF_6, rt).

N′-methylurea dimer $(\mathbf{Upy^{Me}})_2$ (Chart 3). Calculated vibrational spectra are in excellent agreement with the experimental ones as is shown in Table 2. A comparison of the vibrational frequencies calculated for the $(\mathbf{Upy^{Me}})_2$ dimer with those of the $\mathbf{Upy^{Me}}$ monomer indicates that hydrogen bonding induces a sizable red-shift of the vibration formed by the combined asymmetric stretch $\nu(CO)_{pmd,\ as}$ and the $\delta\ (CNH)_{urea}$ bending mode of about 50 cm^{-1}. This calculated shift does not substantially depend on density functional and quality of the basis set (Table S6 of the Supporting Information). Vibrational analyses on $(\mathbf{Upy^{Me}})_2$ also help in the assignment of the individual IR bands of the Upy-substituted styryl complexes. Plots indicating the atomic motions for every crucial vibration in that spectral region are shown as Figure

Chart 3. Model Compounds Used in the Calculations

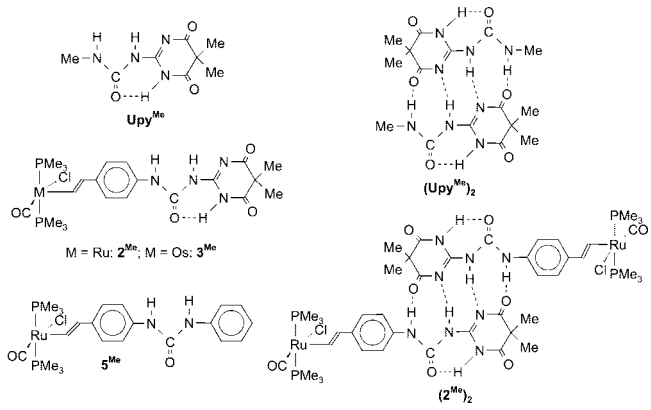

Table 4. G03/B3LYP Calculated Symmetry Averaged Bond Lengths (Å) for Model Complexes $\mathbf{2^{Me}}$ and $\mathbf{5^{Me}}$ and the Comparison with Experimental Ones

	$\mathbf{2^{Me}}$		$\mathbf{5^{Me}}$	
	calculated	experimental	calculated	experimental[a]
Ru−C_1(CO)	1.828	1.820(12)	1.828	1.816(9)
Ru−Cl	2.452	2.432(2)	2.454	2.4622(16)
Ru−P	2.389	2.394(2)	2.389	2.389(2), 2.406(2)
Ru−C_2	2.001	1.985(8)	2.013	2.0007(8)
C_2−C_3	1.349	1.325(12)	1.348	1.302(11)
C_3−C_4	1.473	1.487(11)	1.474	1.429(15)
C_4−C_5	1.408	1.372(12)	1.408	1.431(14), 1.422(12)
C_5−C_6	1.391	1.401(11)	1.389	1.337(16), 1.353(16)
C_6−C_7	1.403	1.369(11)	1.403	1.414(12), 1.409(15)
C_7−N_1	1.417	1.425(10)	1.412	1.433(13)
N_1−C_8	1.372	1.337(10)	1.387	1.370(15)
C_8−N_2	1.441	1.434(10)	1.390	1.329(15)
N_2−C_9	1.381	1.301(10)	1.410	1.421(12)

[a] Data for molecule B.

Chart 4. Numbering Scheme of Table 4

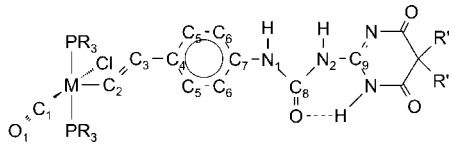

S15 of the Supporting Information. With these assignments at hand it becomes clear that oxidation of the vinyl complexes only affects the energy of the NH bend of the urea nitrogen that is directly attached to the styryl ligand. There is only a negligible shift of all other local vibrators of the urea and pyrimidinedione functionalities that are directly involved in hydrogen bonding. This provides another piece of evidence that these moieties do not contribute to the redox orbitals.

Single-point DFT calculations on the experimental geometry of the dimeric Ru complex $(\mathbf{2^{Me}})_2$ underscore these findings. The highest-lying orbitals HOMO and HOMO−1 are each localized on only one Ru−styryl part and receive only minor contributions from the Upy substituent (see Figure 14). The calculated HOMO of an isolated monomer $\mathbf{2^{Me}}$ is almost identical to that of the corresponding one of the dimeric model species $(\mathbf{2^{Me}})_2$ and of the phenylurea model complex $\mathbf{5^{Me}}$ (Figure 15). The HOMO − HOMO−1 separation of 0.051 eV indicates that electronic coupling[53] between the two monomers is low. Calculated spin densities of $(\mathbf{2^{Me}})_2^{\bullet+}$ (see Table 6, Figure 16)

(53) Newton, M. D. *Chem. Rev.* **1991**, *91*, 767–792.

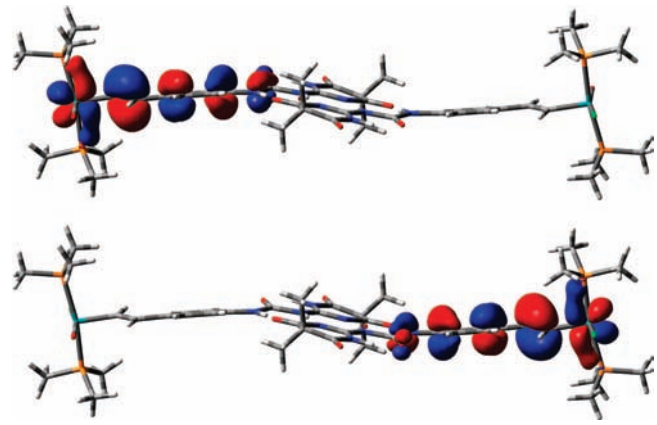

Figure 14. Plots of the HOMO (top) and HOMO−1 (bottom) of the dimeric model complex $(\mathbf{2a^{Me}})_2$.

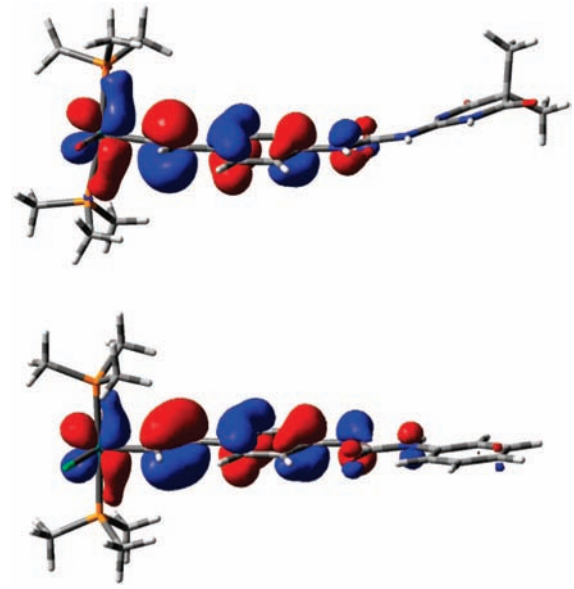

Figure 15. Plots of the HOMOs of monomeric model complexes $\mathbf{2^{Me}}$ (top) and $\mathbf{5^{Me}}$ (bottom).

Table 6. DFT G03/PBE0 Calculated Spin Densities for the Dimeric Model Complex $(\mathbf{2^{Me}})_2^{\bullet+}$ Expressed in Terms of Composing Fragments

	Ru1	Ru2	Et1	Ph1	Cl1	CO1	urea1
spin density	0.437	0.016	0.328	0.183	−0.003	−0.022	0.039

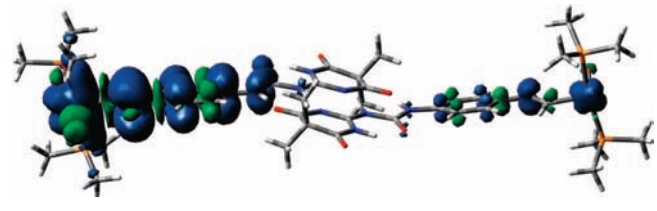

Figure 16. Calculated spin densities for the monooxidized form $(\mathbf{2^{Me}})_2^{\bullet+}$ of the dimeric model complex.

also show that there is very little spin delocalization between individual monomers. The total contribution of the second styryl ruthenium entity is thus only 0.016. Taken together, the quantum chemical results fully agree with those of our experiments in the major point of this study: There is hardly any charge and spin delocalization across the quadruply hydrogen-bonding Upy

motif, at least in the present case of styryl ruthenium and osmium complexes. This leads to valence localization on one of the terminal redox-active styryl ruthenium or osmium subunits in the one-electron oxidized mixed-valent state.

Discussion

Our results indicate efficient electron delocalization within the metal styryl entities of complexes **2a**,**b**, **3a**,**b**, and **5**. From a structural viewpoint we infallibly observe rough coplanarity of the styryl group with the Ru(CO)Cl plane and only a slight rotation of the phenyl ring with respect to the MCH=CH plane. Moreover, the quinoidal distortion of the styryl ring clearly surpasses that of the terminal one in complex **5**. More relevant to the behavior in solution are the first redox potentials of complexes **2a**,**b** (0.19 and 0.195 V), **3a**,**b** (0.020 and 0.015 V), **5** (0.085 V), and of the simple styryl complex $Cl(CO)(P^iPr_3)_2RuCH{=}CHPh$ (0.27 V). The data clearly indicate that the metal *and* the 4-substituent on the phenyl ring exert a strong influence on the redox potential. In contrast, electronic interactions between individual hydrogen bonded styryl metal complexes in dimers $(\mathbf{2a})_2$, $(\mathbf{2b})_2$, $(\mathbf{3a})_2$ and $(\mathbf{3b})_2$ are undetectably small. They neither lead to a splitting of half-wave potentials in electrochemistry nor to an intervalence charge-transfer absorption in electronic spectra as would be expected of even a weakly coupled mixed-valent system of class II. The only indication of such an interaction is the small calculated splitting of the HOMO and HOMO−1 orbitals of the model comples $(\mathbf{2^{Me}})_2$ of 0.051 eV. In addition, none of these systems showed any CO bands besides that of the neutral and that of the dioxidized dicationic forms in IR spectroelectrochemistry even during the electrolysis. Comproportionation equilibria dictate that the corresponding radical cations must be present to some extent in solution besides the neutral and fully oxidized forms. The fact that we cannot detect them simply means that they have no inherent spectroscopic fingerprint different from the neutrals and the dications, i.e. the oxidized or reduced subunits of a mixed-valent dimer have the same $\tilde{\nu}$(CO) as the fully oxidized dications or reduced neutrals, respectively. The seemingly one-step conversions of the neutrals to the dications clearly argue against an even moderate electronic coupling. In the presence of such coupling, two bands at similar but slightly different energies as in the isovalent states should be observed for the intermediate radical cation.[54,55] Even IR changes of the NH···N=C and NH···O=C band pattern upon oxidation are restricted to those urea NH groups that are directly bonded to the styryl moiety.

The monomeric phenylurea derivative **5** produces the same two-wave pattern in electrochemistry with nearly identical splittings of half-wave potentials, the same oxidation-induced CO band shift and similar electronic bands in the oxidized state as the dimeric counterparts. The only difference is that each wave involves just one as opposed to two electrons per wave. Quantum chemistry indicates that conjugation in the present systems extends to the styryl moiety but not beyond. In particular, the NH···*N*=C and NH···O=C moieties that are involved in the hydrogen bonding do not contribute to any of the occupied frontier orbitals. This shuts down on the electronic interactions between the bridged subunits in spite of the high charge and spin densities at the urea-bonded styryl ring as they are typical of ruthenium and osmium styryl complexes. This lets us conclude that in the absence of an electronic driving force for directional electron transfer between a (photo)donor and a (photo)acceptor the quadruply hydrogen-bridging Upy motif is unable to support efficient electronic coupling between the (redox active) styryl ruthenium or osmium end groups. The reasons for the deviating behavior of the analogous ferrocene system remain unclear at this point.

One may, of course, object that our failure to observe any electronic interactions across the Upy bridges of $(\mathbf{2a})_2$, $(\mathbf{2b})_2$, $(\mathbf{3a})_2$, and $(\mathbf{3b})_2$ is simply due to disintegration of the dimers into monomers following oxidation. Our reasoning against such a scenario is as follows: If the oxidation would bring about dissociation into monomers, one might expect indicative changes of the $\nu\ (CO)_{pmd,\ as} + \delta\ (CNH)_{urea}$ vibration mode which, according to our quantum chemical calculations, is highly sensitive to whether the system is monomeric or dimeric in solution. This is, however, not the case. In addition, recent studies on hydrogen bonding between a urea donor and the 1,4-dimethylpiperazine-2,3-dione hydrogen-bond acceptor revealed a >2000-fold binding strength increase upon urea oxidation.[56] Similar arguments should also hold in our case.

Conclusions

Ruthenium and osmium styryl complexes with appended 4,6-dioxo-1,4,5,6-tetrahydropyrimidinylurea (ureapyrimidinedione, Upy) substituents dimerize in an antiparallel arrangement by the quadruple hydrogen bridges of a DDAA (D = hydrogen bond donor, A = hydrogen bond acceptor) motif. The dimeric structures observed in X-ray crystallography are maintained in nonpolar solvents as is shown by the characteristic low-field shifts of the NH protons in NMR spectroscopy. Combined data from conventional electrochemistry, from IR and UV/vis spectroelectrochemistry and from accompanying quantum chemical calculations indicate efficient electron delocalization within the metal styryl subunit of each dimer of complexes $(\mathbf{2a})_2$, $(\mathbf{2b})_2$, $(\mathbf{3a})_2$, and $(\mathbf{3b})_2$ and that of the phenylurea complex **5**, but not beyond. In particular they show that in our case the quadruply hydrogen-bonding motif does not support any detectable electronic coupling between the reduced and oxidized metal styryl subunits. It appears, that the underlying reason is the negligible contribution of the NH···N=C and NH···O=C groups on the urea and pyrimidinedione moieties that are involved in the hydrogen bonding to the occupied frontier orbitals. These findings contrast the highly efficient electron transfer across hydrogen bridges supported by closely related multiply hydrogen-bonded motifs. It also differs from the analogous ferrocene system, whose mixed-valent radical cation seemingly constitutes a borderline class II/III system.[23] The reasons for this dichotomy are presently under investigation by our group.

Acknowledgment. This work is dedicated to Prof. Dr. Otto J. Scherer at the occasion of his 75th birthday. It was generously supported by Deutsche Forschungsgemeinschaft (Grants Wi 1262/7-1 and 436 TSE113/45/0-1) and by the Grant Agency of the Academy of Sciences of the Czech Republic (KAN100400702) and the Ministry of Education of the Czech Republic (Grant COST OC 139). We also thank Dr. Biprajit Sarkar for the recording of the EPR spectrum of partially oxidized $\mathbf{2a}^{\bullet +}$.

(54) Atwood, C. G.; Geiger, W. E. *J. Am. Chem. Soc.* **2000**, *122*, 5477–5485.
(55) Stoll, M. E.; Lovelace, S. R.; Geiger, W. E.; Schimanke, H.; Hyla-Kryspin, I.; Gleiter, R. *J. Am. Chem. Soc.* **1999**, *121*, 9343–9351.
(56) Woods, J. E.; Ge, Y.; Smith, D. K. *J. Am. Chem. Soc.* **2008**, *130*, 10070–10071.

Supporting Information Available: Synthetic procedures and characterization of new compounds and details of the crystal structure determinations and the quantum chemical calculations, figures displaying the crystallographically determined structures of of alkyne **1b** (Figure S1), packing diagrams of alkynes **1b** (Figure S2) and **4** (Figure S11), packing diagrams of complexes **2a** (Figure S3) and **5** (Figure S12), hydrogen-bonding motif with the CH_2Cl_2 solvent of crystallization of complex **2a** (Figure S4); tables with details of the crystal data and structure refinement (Tables S1−S5); tables detailing the calculated vibrations of the model $\mathbf{Upy^{Me}}$ monomer and the $(\mathbf{Upy^{Me}})_2$ dimer (Table S6), TD DFT (G03/B3LYP/CPCM-CH_2Cl_2) calculated lowest lying excitation energies (eV) for $\mathbf{2^{Me}}$(Table S7), $\mathbf{2^{Me\bullet+}}$ (Table S8), $\mathbf{5^{Me}}$ (Table S9) and $\mathbf{5^{Me\bullet+}}$ (Table S10), Figures displaying the ^{1}H NMR spectrum of a CD_2Cl_2 solution of complex **2a** (1.1 mM) in 0.1 M NBu_4PF_6 (Figure S5), the voltammogram of complex **2a** in CH_2Cl_2/MeOH (Figure S6), the ^{1}H NMR spectrum of a mixture of complexes **2a** and **3b** in CD_2Cl_2 at various temperatures (Figure S7), IR spectroscopic changes upon the first (Figure S8) and second (Figure S10) oxidation of complex **2b** and in the NH region of complex **2a** (Figure S9) and complex **5** (Figure S13), the calculated ground-state structure of the $(\mathbf{Upy^{Me}})_2$ dimer (Figure S14) and calculated atom displacements during the vibrations of model complex $(\mathbf{Upy^{Me}})_2$ in the 1750−1500 cm^{-1} region (Figure S15). This material is available free of charge via the Internet at http://pubs.acs.org.

JA809566G